



Computational Study on Aerodynamic Characteristics and Behaviour of S5010 Airfoil

Open
Access

Muhamad Hasfanizam Mat Yazik¹, Masaaki Tamagawa², Mohamed Thariq Hameed Sultan^{1,3,4,*}, Adi Adzrif¹

¹ Department of Aerospace Engineering, Faculty of Engineering, Universiti Putra Malaysia, 43400 UPM Serdang, Selangor Darul Ehsan, Malaysia

² Graduate School of Life Science and Systems Engineering, Kyushu Institute of Technology, 2-4 Hibikino, Wakamatsu-ku, Kitakyushu 808-0196, Japan

³ Laboratory of Biocomposite Technology, Institute of Tropical Forestry and Forest Products (INTROP), Universiti Putra Malaysia, 43400 UPM Serdang, Selangor Darul Ehsan, Malaysia

⁴ Aerospace Malaysia Innovation Centre (944751-A), Prime Minister's Department, MIGHT Partnership Hub, Jalan Impact, 63000 Cyberaya, Selangor Darul Ehsan, Malaysia

ARTICLE INFO

ABSTRACT

Article history:

Received 17 June 2019

Received in revised form 12 December 2019

Accepted 9 January 2020

Available online 26 February 2020

In this study, a numerical simulation has been conducted to understand the effect of angle of attack on the S5010 airfoil profile. ANSYS Fluent was utilized with the compliment of experimental data from literature. The 2-D computational fluid dynamic simulation were conducted to find the lift, drag and lift-to-drag ratio of S5010 airfoil at various angle of attack up till the stalling point. The k- ω SST turbulent model was used to model the turbulent flow during the simulation. The data obtained was compared with available experimental data for validity and later extended to obtain stall angle of the airfoil. It was found that the stall angle of S5010 airfoil was at 11° and the maximum lift-to-drag ratio was obtained at 7.8°. Considering the simulation, acceptable solution has been achieved that can be used to compare with other airfoil profile in the future.

Keywords:

S5010; airfoil; CFD; lift coefficient; drag coefficient; lift-to-drag ratio

Copyright © 2020 PENERBIT AKADEMIA BARU - All rights reserved

1. Introduction

The world is moving towards sustainable energy in term of renewable and efficient energy. Demanding fuel problem is a serious problem nowadays. Greenhouse gasses is one of the big factors contributing to global warming. The aviation industry account for 4.9% of greenhouse gasses [1]. Boeing predict an annual growth of 4.7% in world traffic flow from 2018 to 2037 [2]. Immediate substitute to the fossil fuels is not readily available yet. Biofuels are promising alternatives, but it is unlikely to replace standard fossil fuels for the next several decades. This leaves fuel efficiency improvements as a vital options [3]. Improving fuel efficiency is not only vital for the environment, but also from economical point of view, with an increase of fuel price of about 22% from a year ago [4], airline need more fuel efficient aircraft given the expected grow in traffic flow. More emphasis is

* Corresponding author.

E-mail address: thariq@upm.edu.my (Mohamed Thariq Hameed Sultan)

given in creating more efficient aircraft rather than high performing aircraft [5]. Previously, emphasis were given on creating engine with highest efficiency in order to create high efficiency aircraft [6-7]. Only a small improvement was made in order to improve aircraft wing. Aircraft wing plays an important role in generating lift force and associated drag force which oppose aircraft motion [8]. The cross-section shape of the wing, known as airfoil, is highly investigated in order to improve the lift and drag performance of the wing. Research on which air foil shape is the most suitable for each aircraft are crucial in developing high efficiency aircraft.

The difficulty in designing aircraft wing lies in the testing and validation aspect of design process. Over the last few decades, designers depend on wind tunnel testing in order to validate the wing designed based on research [9]. Wind tunnel model of a wing were created and tested in wind tunnel to confirm the performance of each design. This procedure was costly, exhaustive and time consuming which inspired designers to develop computation fluid dynamics [10]. Through computational method, the fluid flow around air foil can be calculated to predict the aerodynamic characteristics and performance new designs. However, high computational power and sources are required to enable correct prediction. With increasing research on computational research and large collection of database, computational fluid dynamics has becoming more reliable for researchers to examine their design [11-12]. Nowadays, with the advancement of computational codes enable researchers to conduct computational simulation for each air foil designs.

In order to obtain aerodynamically optimum airfoil, the aerodynamic characteristic has to be determined. Traditionally, this was done with experimental wind tunnel. With computational aid, properties such as lift, drag and lift-to-drag ratio of the air foil can be obtained. Turbulence model would play an empirical role in obtaining a correct prediction of aerodynamic characteristics. Over the last few decades, the Spalart-Allmaras turbulence model has been used extensively in the industry to predict flow around an airfoil [13-14]. However, this model unable to successfully capture the flow dynamics of turbulence at low Reynold number as this flow is highly dominated by turbulence phenomena. In the last decade, the k- ω SST model has proven to be reliable in predicting the fluid flow around an external flow which includes flow around airfoil [15-19]. Ahmed *et al.*, [20] did a simulation study of pitching NACA0012 air foil using various turbulence model and found out that k- ω SST provide the best prediction with respect to experimental data with Y^+ set to 1.

For relatively common airfoil, such as NACA airfoil, the aerodynamic characteristics is well known and frequently studied thus the aerodynamic data are vastly available and accessible. However, for specifically designed airfoil, limited data available regarding its behaviour. Selig 5010 airfoil was designed by Michael Selig and Dave Jones for tailless planform and first introduced in 1987 [21]. The airfoil were designed for flying wing aircraft and have positive pitching moment. The wind tunnel data are available from Silvestre *et al.*, [22] however limited computational analysis was performed on this airfoil. In recent years, the importance of tailless aircraft has grown a lot as it seems to improve performance and reduce fuel consumption [23] thus spark the interest in Selig airfoil.

In this paper, a study of aerodynamic characteristics was conducted by computational fluid dynamic simulation using the k- ω SST model. The lift and drag coefficient as well as pressure and velocity variation on the surface of the S5010 airfoil at different angle of attack is studied for a constant Reynolds number. Crucial aerodynamic point such as maximum lift and maximum efficiency angle of attack are determined. Existing approach of the aerodynamic characteristics of S5010 airfoil through experiments were compared in order to obtain a reliable result. The simulation was extended to higher angle of attack further than the stall angle. In this paper, the reliability analysis in the turbulence model were studied.

2. Methodology

2.1 Numerical Analysis

This study was conducted using Ansys Fluent 18.2 supplemented by the data from Low Speed Airfoil Data (experimental data from University of Illinois [22,24]). The S5010 airfoil was designed by Prof. Michael Selig dedicated to tailless and flying wing aircraft in which the zero-pitching moment coefficient was highly desirable. The airfoil has thickness of 9.8% at 27.6% chord. Recently, Mat Yazik *et al.*, [25] study the S5010 profile for blended wing body wing. Meanwhile, Dehpanah and Nejat [26] adapt the S5010 airfoil for preliminary design of blended wing body configuration. A unit airfoil model was created by importing points file into the Ansys Design Modeler and generate surface. The model was then imported into ICEM module to create mesh around the airfoil. The surface domain was shown as in Figure 1.

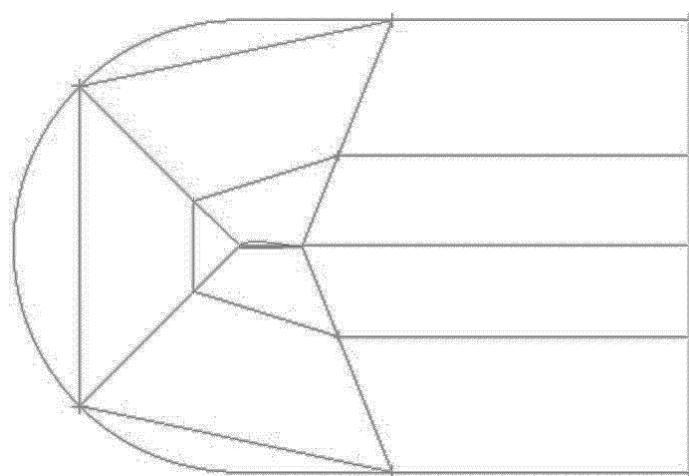


Fig. 1. Fluid domain around airfoil

2.2 Domain Detail

An airfoil with sharp trailing edge with chord length $c = 1.0m$ was created. The fluid domain around the airfoil consist of a semicircle which is classified as inlet before the airfoil and a rectangular which is classified as outlet after the airfoil. The inlet was kept at $4c$ distance from the leading edge of the airfoil and the outlet were kept at $10c$ after the trailing edge of the airfoil. The fluid domain above and below the airfoil were kept at $4c$ distance to avoid wall effect on the flow around the airfoil. Meshing were carried out using ICEM module incorporating blocking function and zones discretization of the fluid domain. A C-mesh type of mesh was created due to the sharp trailing edge of the airfoil as can be seen in Figure 2. The meshes zone closer to the airfoil surface were created by layer of fine mesh increasing in size with respect to the distance from airfoil surface (Figure 2 inside). Quadrilateral mesh was created with appropriate first layer distance in order to obtain $Y^+ \leq 1$.

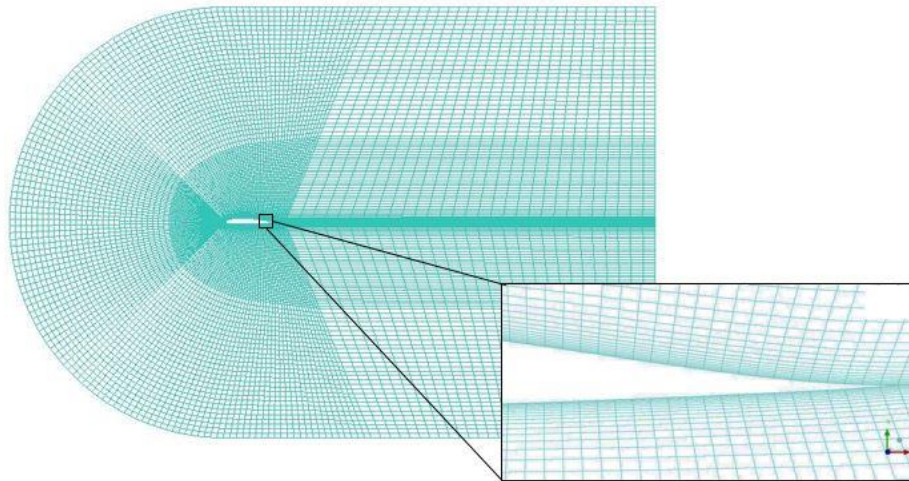


Fig. 2. C-Mesh type around airfoil. In the box: Mesh around the trailing edge

2.3 Boundary Condition

A standard flow condition was used in the simulation according to Silvestre *et al.*, [22] thus the following values of pressure, density and kinematic viscosity were utilized where $P = 101.3 \text{ kPa}$, $\rho = 1.225 \text{ kgm}^{-3}$ and $\nu = 1.79 \times 10^{-5} \text{ m}^2\text{s}^{-1}$ respectively. The inlet flow velocity was set a $Re = 200,000$ based on a unit chord. The inlet turbulent intensity was set to 0.2% with respective length scale at third of the chord. The inlet boundary consists of the semi-circular as well as top and bottom wall of the airfoil. Incompressible flow was assumed as the flow was in low Re number thus a pressure-based solver was used, implementing SIMPLE pressure velocity coupling. Second-order discretization was used for pressure, momentum, turbulent dissipation energy and turbulent dissipation rate. The convergence criteria were set to 1×10^{-4} and the angle of attack simulated ranges from approximately -4.91° to 13.3° in order to show the stalling effect of the airfoil.

2.4 $k-\omega$ Model

The $k-\omega$ model is a two equation model developed by Wilcox [27]. It incorporates modifications for low Reynolds number effects, compressibility and shear flow spreading. The $k-\omega$ model predicts free shear flow spreading rates, thus is applicable to wall-bounded flows and free shear flows. It has better accuracy and reliable stability for a wide range of flows. The $k-\omega$ model comes in two variants, which are the standard $k-\omega$ model and the shear-stress transport (SST) $k-\omega$ model [15,28]. The SST $k-\omega$ model effectively blends the standard $k-\omega$ model with the $k-\epsilon$ model [29]. This is done by multiplying both models with a blending function and adding both models together, ensuring a smooth transition between the two models [30]. The blending function activates the $k-\omega$ model for the near-wall region and zero away from the surface, subsequently activates the $k-\epsilon$ model. The SST $k-\omega$ model's turbulent viscosity is defined to accommodate the transport of principal turbulent shear stress. The transport equations for the SST $k-\omega$ model are as follows.

$$\frac{\partial}{\partial t}(\rho k) + \frac{\partial}{\partial x_i}(\rho k u_i) = \frac{\partial}{\partial x_j} \left[\Gamma_\omega \frac{\partial k}{\partial x_j} \right] + G_k - Y_k + S_k \quad (1)$$

$$\frac{\partial}{\partial t}(\rho \omega) + \frac{\partial}{\partial x_i}(\rho \omega u_i) = \frac{\partial}{\partial x_j} \left[\Gamma_\omega \frac{\partial \omega}{\partial x_j} \right] + G_\omega - Y_\omega + D_\omega + S_\omega \quad (2)$$

where

G_k = generation of turbulence kinetic energy due to mean velocity gradients

G_ω = generation of ω

Γ_k and Γ_ω = effective diffusivity of k and ω , respectively.

While

Y_k and Y_ω = dissipation due to turbulence of k and ω , respectively.

D_ω = cross-diffusion term and

S_k and S_ω = user-defined source terms.

2.5 Mesh Independence Check

A mesh independency was conducted prior to the study in order to obtain numerical result independent of the mesh number. The test was conducted by varying the number of nodes in the central region of the fluid domain. The nodes in each zone were controlled by increasing the number of divisions on each line. A point downstream was set as a reference point as a criterion for mesh independency. A graph of monitored properties as a function of mesh number is shown in Figure 3. As can be seen, low mesh number produce large deviation from a stable value. High mesh number gives smaller variation due to higher accuracy however, higher mesh number requires large computational power and take longer to converge thus an optimized number of mesh is selected with acceptable solution for the rest of the study. A solution produced above 100k elements produced stable solution while increasing the mesh number would result in slight change in converged solution. Thus, a mesh number of 132k mesh was selected for the rest of the study.

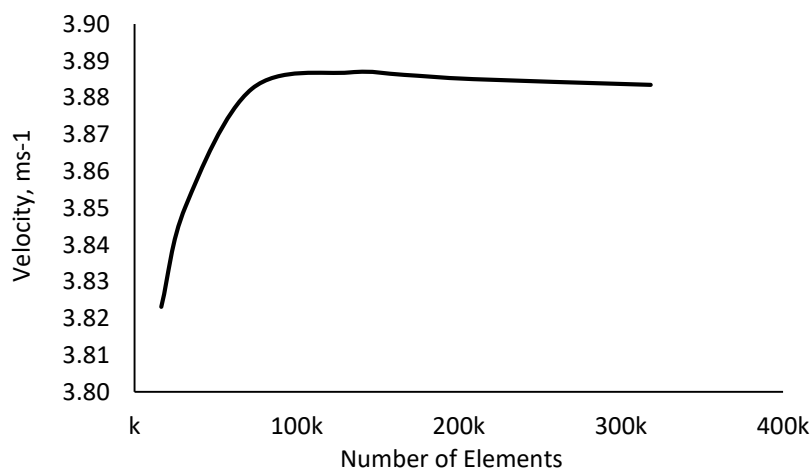


Fig. 3. Monitored velocity against Number of elements for mesh independency study

3. Results

3.1 Aerodynamic Properties

The lift and drag of the airfoil calculated within the Ansys at -4.91° and 8.92° angle of attack are compared against experimental data. The drag and lift coefficient of were defined as following.

$$C_d = \frac{d}{\rho v^2 \frac{A}{2}} \quad (3)$$

$$C_l = \frac{l}{\rho v^2 \frac{A}{2}} \tag{4}$$

Where d, l, ρ, v and A are drag, lift, fluid density, flow velocity and area respectively. The lift and drag coefficients were calculated by integration of the pressure values on the wing surface.

In order to verify the validity of the simulation and calculation result, the lift and drag of the simulated result were compared with existing experimental data from Silvestre *et al.*, [22]. As shown in Table 1, the simulation data for lift and drag has error of about 7.59% and 3.86% respectively for -4.91° and 4.25% and 29.24% respectively for 8.92°. This error is still within the general acceptable limit of simulation error of less than 30%.

Table 1
 Comparison of data from experimental and computational

Angle of Attack	Lift		Drag	
	4.91°	8.92°	4.91°	8.92°
Experimental	-0.395	0.977	0.0339	0.0203
Simulation	-0.3649	1.101	0.03259	0.0262
% Error	7.59	4.25	3.86	29.24

Figure 4 shows the variation of lift and drag of S5010 airfoil at various angle of attack from -4.91° to 13.3°. From the simulated data, we can see confirm that the lift coefficient increases rapidly with proportional with angle of attack. The lift coefficient, however, fall rapidly after approximately 11°. At this point, the stall occurs. At this value, the maximum lift coefficient is 1.1403 in which the value drops beyond the stall angle. As can be see, the drag coefficient is significantly lower than the lift coefficient. However, near stall angle, the drag coefficient increases as a result of drag generated due to separation over the airfoil surface. Increasing the angle of attack induces separation over the airfoil's upper surface. As the angle of attack keep increasing, the point of separation is nearer to the leading edge thus creating higher drag. The drag coefficient at stall angle 11° is 0.04581 and the drag coefficient at 13.3° is 0.07788 which is the highest than at any angle of attack. The drag coefficient is the lowest near 0° in which the drag is near zero. After approximately 8°, the drag coefficient starts to increase significantly as can be seen in Figure 4.

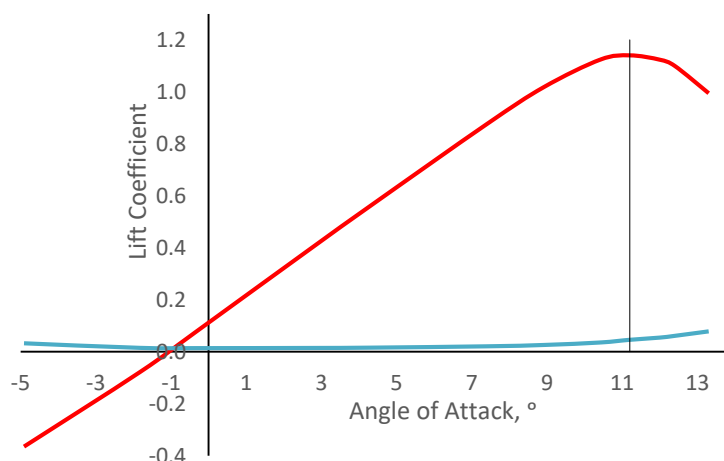


Fig. 4. Lift and drag coefficient of S5010 against angle of attack

Figure 5 shows the lift-to-drag ratio at various angle of attack of the S5010 airfoil. Lift-to-drag ratio is assumed to be the measure of airfoil profile efficiency because it involves both aerodynamic

characteristics which is lift and drag. The higher the lift-to-drag ratio, the more efficient the airfoil. The maximum lift-to-drag ratio indicate that the lift generated at that angle of attack is larger compared to the drag generated at that same angle. From the simulation, the maximum lift-to-drag ratio was found to be at 7.8° with lift-to-drag ratio of about 41.58. For this airfoil, the angle of attack at 7.8° is the most efficient angle where high lift was generated with low associated drag.

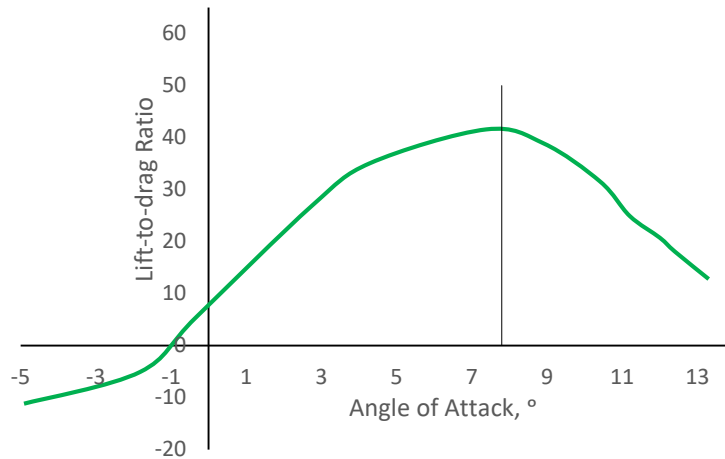
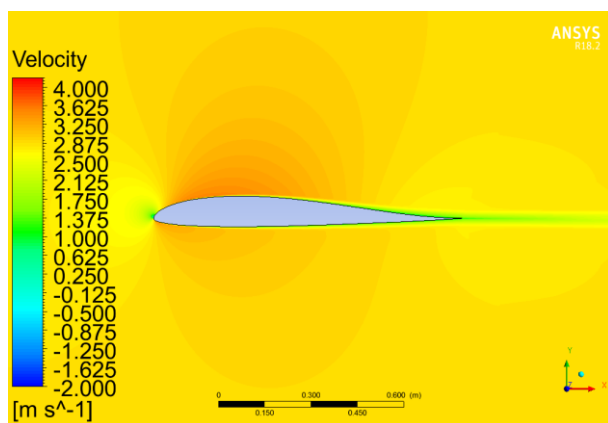


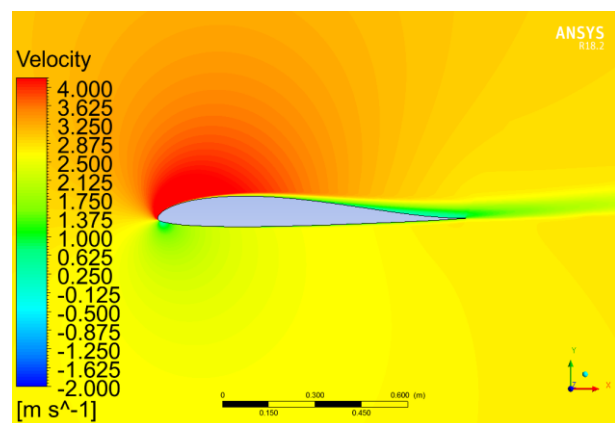
Fig. 5. Lift-to-Drag ratio of S5010 airfoil against angle of attack

3.2 Velocity Contour

As can be seen in Figure 6, the velocity around the airfoil gradually increase as the angle of attack increase. The velocity on the upper surface is greater than the lower surface as an effect of surface curvature of the upper surface. The difference in fluid velocity creates a different in pressure around the airfoil. It can be observed that the velocity of fluid at the trailing edge is gradually reduced as the angle of attack is increased. This is due to the effect of adverse pressure effect between the upstream and downstream pressure which causes the fluid travelling along the airfoil to slow down. This is usually associated with flow separation which increase drag.



(a)



(b)

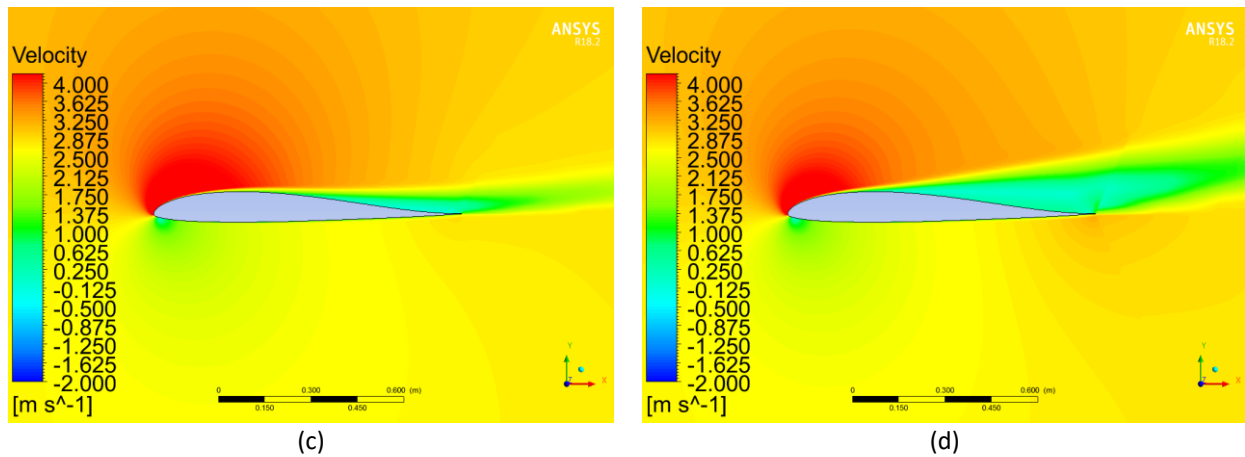


Fig. 6. Contour of fluid velocity around S5010 airfoil at various angle of attack. a) 0° b) 7.8° c) 11° and d) 13.3°

3.3 Pressure Contour

From Figure 7 we can see that the pressure difference above and below the airfoil also increase as the angle of attack increase. At 11°, the pressure difference is the largest compared to others. This generates the highest lift as shown before in Figure 4. The pressure difference beyond 8° decrease as the airfoil produces smaller difference in pressure due to flow separation.

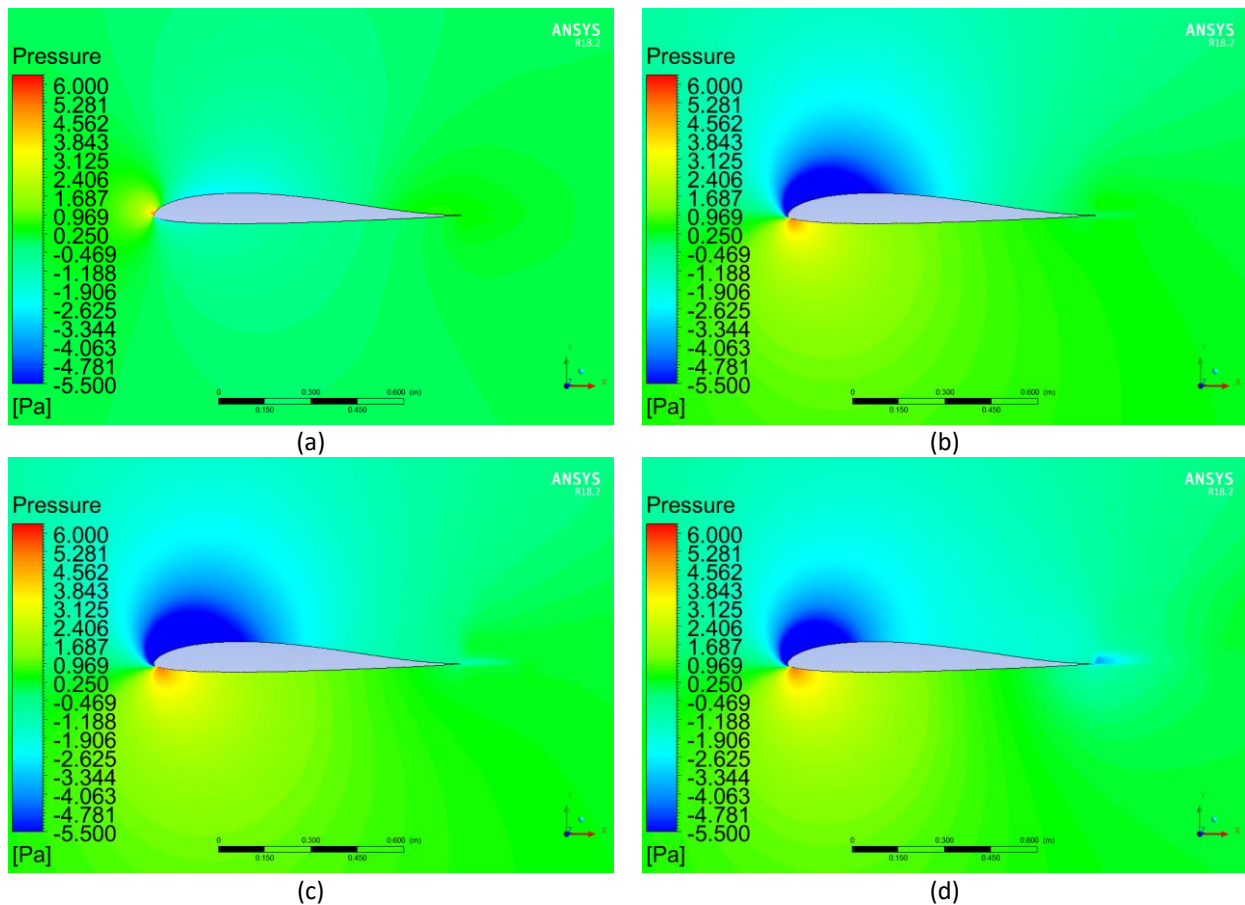


Fig. 7. Contour of pressure around S5010 airfoil at various angle of attack. a) 0° b) 7.8° c) 11° and d) 13.3°

As mentioned before, there is a high possibility of flow separation at high angle of attack. This is because the airflow was unable to follow the curvature of the airfoil surface. The difference in pressure behind the trailing edge and in front of the leading edge encourage the separation and induce a secondary flow within the boundary layer as well.

3.4 Velocity Streamline

Figure 8 shows the velocity streamline of air around the airfoil. As can be seen, separation point moves along the upper surface towards the leading edge as angle of attack increase. Separation occurs due to high pressure gradient between the trailing edge and leading edge as shown before. This pushes the airflow towards the leading edge of the airfoil. At a certain point, the flow will detach from the surface of the airfoil and begin flowing in reverse direction creating a secondary flow within the flow itself [31]. This effect is more prominent at high angle of attack as the possibility of separation is higher. In Figure 8(d), there is an obvious secondary flow occurring above the airfoil surface. This creates a vortex of flows which extends until the trailing edge. As seen in Figure 4, the drag increase significantly as a result of flow separation. This shows the importance a suitable airfoil which can keep the flow attached as further as possible in order to reduce the drag associated with it.

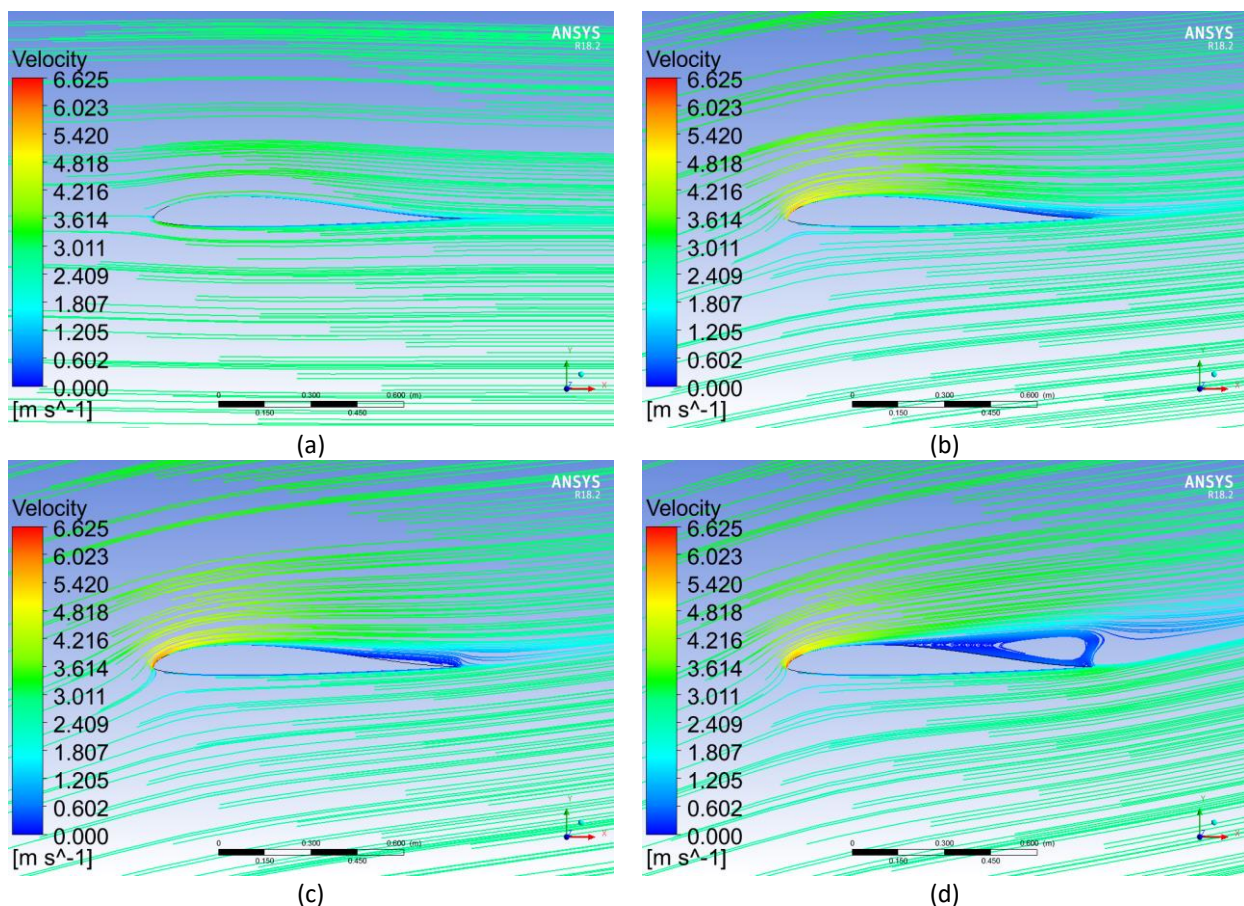


Fig. 8. Velocity streamline around the airfoil at a) 0° b) 7.8° c) 11° and d) 13.3°

4. Conclusions

In this present study, the aerodynamic properties of S5010 airfoil was studied using computational fluid dynamic method via the ANSYS package. The lift and drag coefficient as well as lift-to-drag ratio was simulated at various angle of attack using the k- ω SST turbulent model. The result of the simulated data was compared, and the error were calculated which turn out to be within the acceptable range. For further study, various turbulent model can be considered as the turbulent flow highly influence the flow at low Reynold number. Various shape of airfoil can also be studied in order to find a more suitable airfoil. The current study was summarized as following:

- i. Lift and drag coefficient depend on the angle of attack where the effect is more prominent on the lift coefficient.
- ii. Maximum lift (stall) occur at 11° with lift coefficient of 1.1403 in which the value drops rapidly after stall angle of attack.
- iii. The drag coefficient is the lowest near 0° and increase as the angle of attack increase.
- iv. The maximum lift-to-drag ratio is obtained at 7.8° angle of attack.

Acknowledgement

This work is supported by UPM under GP-IPS grant, 9647200. The authors would like to express their gratitude and sincere appreciation to the Department of Aerospace Engineering, Faculty of Engineering, Universiti Putra Malaysia and Laboratory of Biocomposite Technology, Institute of Tropical Forestry and Forest Products (INTROP), Universiti Putra Malaysia (HiCOE) for the close collaboration in this research).

References

- [1] Lee, David S., David W. Fahey, Piers M. Forster, Peter J. Newton, Ron CN Wit, Ling L. Lim, Bethan Owen, and Robert Sausen. "Aviation and global climate change in the 21st century." *Atmospheric Environment* 43, no. 22-23 (2009): 3520-3537.
- [2] Boeing. "Commercial Market Outlook 2018–2037." (2018).
- [3] Walker, Gabrielle, and David King. *The hot topic: what we can do about global warming*. Houghton Mifflin Harcourt, 2008.
- [4] <https://www.iata.org/en/publications/economics/fuel-monitor/>
- [5] Lee, Joosung J. "Can we accelerate the improvement of energy efficiency in aircraft systems?." *Energy conversion and management* 51, no. 1 (2010): 189-196.
- [6] Greene, David L. "Energy-efficiency improvement potential of commercial aircraft." *Annual review of energy and the environment* 17, no. 1 (1992): 537-573.
- [7] Lee, Joosung J., Stephen P. Lukachko, Ian A. Waitz, and Andreas Schafer. "Historical and future trends in aircraft performance, cost, and emissions." *Annual Review of Energy and the Environment* 26, no. 1 (2001): 167-200.
- [8] Antoine, Nicolas E., and Ilan M. Kroo. "Framework for aircraft conceptual design and environmental performance studies." *AIAA journal* 43, no. 10 (2005): 2100-2109.
- [9] Johnson, Forrester T., Edward N. Tinoco, and N. Jong Yu. "Thirty years of development and application of CFD at Boeing Commercial Airplanes, Seattle." *Computers & Fluids* 34, no. 10 (2005): 1115-1151.
- [10] Malik, Murjeeb R., and Dennis M. Bushnell. "Role of computational fluid dynamics and wind tunnels in aeronautics r and d." (2012).
- [11] Fujii, Kozo. "Progress and future prospects of CFD in aerospace—Wind tunnel and beyond." *Progress in Aerospace Sciences* 41, no. 6 (2005): 455-470.
- [12] Slotnick, Jeffrey, Abdollah Khodadoust, Juan Alonso, David Darmofal, William Gropp, Elizabeth Lurie, and Dimitri Mavriplis. "CFD vision 2030 study: a path to revolutionary computational aerospace." (2014).
- [13] Spalart, Philippe, and Steven Allmaras. "A one-equation turbulence model for aerodynamic flows." In *30th aerospace sciences meeting and exhibit*, p. 439. 1992.
- [14] Kunya, Bashir Isyaku, Clement Olaloye Folayan, Gyang Yakubu Pam, Fatai Olukayode Anafi, and Nura Mu'az Muhammad. "Performance study of Whale-Inspired Wind Turbine Blade at Low Wind Speed Using Numerical Method." *CFD Letters* 11, no. 7 (2019): 11-25.

- [15] Menter, Florian R. "Two-equation eddy-viscosity turbulence models for engineering applications." *AIAA journal* 32, no. 8 (1994): 1598-1605.
- [16] Menter, Florian R., Martin Kuntz, and Robin Langtry. "Ten years of industrial experience with the SST turbulence model." *Turbulence, heat and mass transfer* 4, no. 1 (2003): 625-632.
- [17] Muhammad Syahmi Abdul Hakim, Mastura Ab Wahid, Norazila Othman, Shabudin Mat, Shuhaimi Mansor, Md. Nizam Dahalan, and Wan Khairuddin Wan Ali. "The effects of reynolds number on flow separation of Naca Aerofoil." *Journal of Advanced Research in Fluid Mechanics and Thermal Sciences* 47, no. 1 (2018): 56-68.
- [18] Jaffar Syed Mohamed Ali, and M. Mubin Saleh. "Experimental and Numerical Study on the Aerodynamics and Stability Characteristics of a Canard Aircraft." *Journal of Advanced Research in Fluid Mechanics and Thermal Sciences* 53, no. 2 (2019): 165-174.
- [19] Ang, Jia Hui, Yusri Yusup, Sheikh Ahmad Zaki, Ali Salehabadi, and Mardiana Idayu Ahmad. "CFD Study on the Behaviour and Turbulence of the Airflow Induced by The Moving Elevator Car in Elevator Shaft Using K-Epsilon Model." *CFD Letters* 11, no. 11 (2019): 1-12.
- [20] Ahmad, KA Ahmad KA, MZ Abdullah MZ Abdullah, and JK Watterson JK Watterson. "Numerical modelling of a pitching airfoil." *Jurnal Mekanikal* 30, no. 1 (2010).
- [21] G. A. Dees. "SoarTech The Flying Wing Edition." *Soartech Journal* 7, (1987): 1-120.
- [22] Selig, Michael S. *Summary of low speed airfoil data*. SOARTECH publications, 1995.
- [23] Milani, Maurizio. "Aerodynamic shape optimization of tailless aircraft." Master Thesis, POLITECNICO DI MILANO, 2016.
- [24] Lyon, Christopher Alan. "Summary of low-speed airfoil data." PhD diss., University of Illinois at Urbana-Champaign, 2001.
- [25] Yazik, MH Mat, M. T. H. Sultan, and A. Hamdan. "Wing design for blended-wing-body aircraft." *Proceedings of Mechanical Engineering Research Day 2017* 2017 (2017): 142-143.
- [26] Dehpanah, Payam, and Amir Nejat. "The aerodynamic design evaluation of a blended-wing-body configuration." *Aerospace Science and Technology* 43 (2015): 96-110.
- [27] Wilcox, David C. "Reassessment of the scale-determining equation for advanced turbulence models." *AIAA journal* 26, no. 11 (1988): 1299-1310.
- [28] Menter, Florian R. "Influence of freestream values on k-omega turbulence model predictions." *AIAA journal* 30, no. 6 (1992): 1657-1659.
- [29] Jones, W. P., and Brian Edward Launder. "The prediction of laminarization with a two-equation model of turbulence." *International journal of heat and mass transfer* 15, no. 2 (1972): 301-314.
- [30] Wilcox, David C. *Turbulence modeling for CFD*. Vol. 2. La Canada, CA: DCW industries, 1998.
- [31] Merryisha, Samuel, and Parvathy Rajendran. "Experimental and CFD Analysis of Surface Modifiers on Aircraft Wing: A Review." *CFD Letters* 11, no. 10 (2019): 46-56.